Single-crystal neutron diffraction study of short-range magnetic correlations in Tb_5Ge_4

W. Tian,[1,2] A. Kreyssig,[1,2] J. L. Zarestky,[1,2] L. Tan,[1,2] S. Nandi,[1,2] A. I. Goldman,[1,2] T. A. Lograsso,[2] D. L. Schlagel,[2] K. A. Gschneidner,[2,3] V. K. Pecharsky,[2,3] and R. J. McQueeney[1,2]

[1]*Department of Physics and Astronomy, Iowa State University, Ames, Iowa 50011, USA*

[2]*Ames Laboratory, U.S. DOE, Iowa State University, Ames, Iowa 50011, USA*

[3]*Department of Materials Science and Engineering, Iowa State University, Ames, Iowa 50011, USA*

(Received 17 August 2009; revised manuscript received 2 October 2009; published 28 October 2009)

We present a single-crystal neutron diffraction study of the magnetic short-range correlations in Tb_5Ge_4 which orders antiferromagnetically below the Neel temperature $T_N \approx 92$ K. Strong diffuse scattering arising from magnetic short-range correlations was observed in wide temperature ranges both below and above T_N. The antiferromagnetic ordering in Tb_5Ge_4 is described to consist of strongly coupled ferromagnetic block layers in the *ac* plane that stack along the *b* axis with weak antiferromagnetic interlayer coupling. Diffuse scattering was observed along both a^* and b^* directions indicating three-dimensional short-range correlations. Moreover, the *q* dependence of the diffuse scattering is Squared Lorentzian in form suggesting a strongly clustered magnetic state that may be related to the proposed Griffiths-like phase in Gd_5Ge_4.

DOI: 10.1103/PhysRevB.80.134422 PACS number(s): 75.40.Cx, 75.30.Sg, 75.50.Ee

I. INTRODUCTION

Tb_5Ge_4 and Gd_5Ge_4 belong to the rare earth $R_5(Si_xGe_{1-x})_4$ series compounds. These materials exhibit large magnetocaloric (MC) effects[1–4] and are currently attracting much attention for their potential application in magnetic refrigeration.[2,5–7] Both Tb_5Ge_4 and Gd_5Ge_4 are rich in magnetic properties[8–16] and are believed to play a key role in understanding the underlying physics of the $R_5(Si_xGe_{1-x})_4$ systems. They both crystallize in the Sm_5Ge_4-type crystallographic structure and adopt the same magnetic space group, $Pnm'a$.[15,17,18] Tb_5Ge_4 and Gd_5Ge_4 undergo long range antiferromagnetic (AFM) transitions at ~92 K and ~127 K, respectively. The magnetic structure of Tb_5Ge_4 and Gd_5Ge_4 consist of Tb/Gd-rich block layers in the *ac* plane that stack along the *b*-axis with strong ferromagnetic intralayer and weak AFM interlayer interactions. Gd_5Ge_4 has a collinear AFM structure with the magnetic moments lying within the block layers along the *c* axis. Tb_5Ge_4 orders in a similar fashion, although the single-ion anisotropy results in significant canting of the moments at low temperature.

Figure 1 shows the magnetic susceptibility of Tb_5Ge_4 along all three crystallographic axes measured with a quantum design SQUID magnetic properties measurement system. The inset of Fig. 1 depicts the temperature dependence of the inverse magnetic susceptibility. It follows Curie-Weiss behavior above 160 K with similar slope for all three crystallographic directions. The derived Curie constant of 58.8 cm^3 K/mol results in an effective paramagnetic moment of $\mu^{eff}=9.7$ μ_B close to the theoretical value 9.72 μ_B for a free Tb^{3+} ion. The paramagnetic Curie temperatures are about ~25 K along both *a* axis and *c* axis pointing to dominating ferromagnetic coupling in the *ac* plane. On the other hand, the paramagnetic Curie temperature along the *b* axis is about ~−50 K indicating dominating antiferromagnetic interaction along this direction. These couplings are consistent with the reported magnetic order in Tb_5Ge_4.[15] Two phase transitions were observed in the magnetic susceptibility measurements: the AFM transition at $T_N \sim 92$ K and a second phase transition at ~55 K. The ~55 K transition was attributed to a spin reorientation transition[7,15] [a weak anomaly observed in the electrical resistivity and a x-ray resonant magnetic scattering measurement of Gd_5Ge_4 at ~75 K (Ref. 19) was proposed to be associated with a spin reorientation transition similar to Tb_5Ge_4]. It has been suggested that the spin reorientation transition in Tb_5Ge_4 may arise from the delicate competition between the magnetic anisotropy from the spin-orbit coupling of the conduction electrons and the dipolar interaction anisotropy.[19] In addition to the AFM and spin reorientation transitions, it is of particular interest that significant magnetic short-range correlations (SRC) was suggested in Gd_5Ge_4 at temperatures both below and above T_N based upon the low magnetic field dc magnetization and ac magnetic susceptibility measurements.[12] It has been interpreted as evidence of a Griffiths-like phase similar to the one

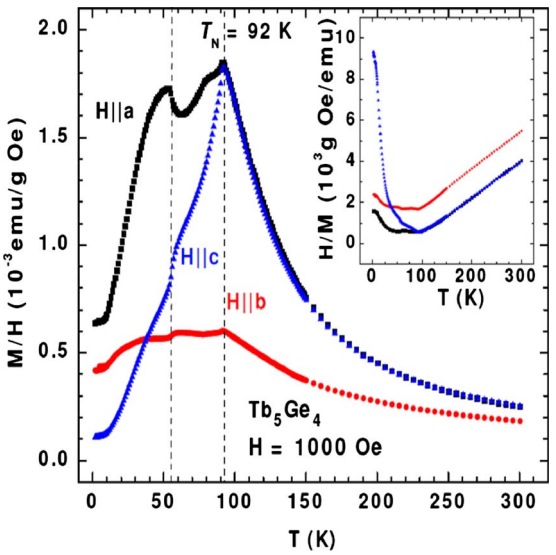

FIG. 1. (Color online) Temperature dependencies of the magnetic susceptibility (Inset: inverse magnetic susceptibility) measured with applied magnetic field (H=1000 Oe, zero-field cooled) parallel to all three crystallographic axes.

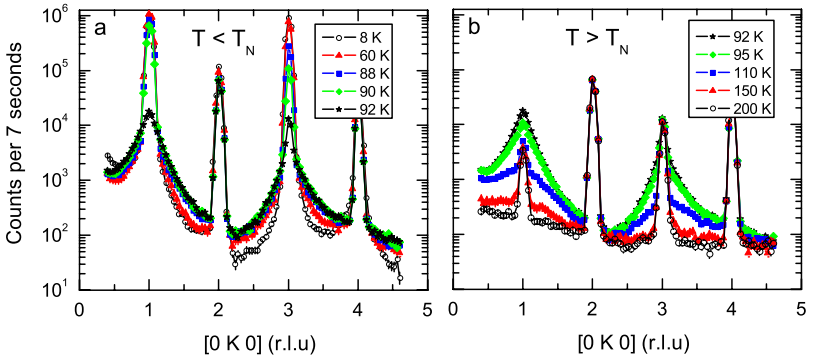

FIG. 2. (Color online) Longitudinal scans (in Log10 scale) along the $(0k0)$ direction measured at several temperatures (a) below T_N, (b) above T_N, indicate strong AFM SRC with broad magnetic scattering observed around k=odd. The remaining scattering intensity of (010) and (030) at 200 K is likely due to multiple scattering.

observed in $Tb_5Si_2Ge_2$, investigated by small-angle neutron scattering.[16] A Griffiths phase[20] is a nanoscale magnetic clustering phenomenon that is usually associated with competing magnetic interactions in the system.[21–23] It is possible for a Griffiths-like phase to exist in Gd_5Ge_4 due to the competition between FM and AFM interactions in Gd_5Ge_4, FM interactions within the layers, and either AFM or FM interactions between the layers (small structural changes or applying relatively low magnetic field comparing to T_N can switch the interlayer interactions between AFM and FM interactions therefore switch the low-temperature phase between AFM order or FM order). However, studies of Gd_5Ge_4 have been hampered by the large neutron absorption cross-section of gadolinium. Tb_5Ge_4 exhibits similar magnetic properties as to Gd_5Ge_4 hence it is an ideal candidate for neutron-scattering studies of magnetic SRC displayed in these compounds. We report here neutron diffraction studies of the AFM phase transition and the magnetic SRC in Tb_5Ge_4.

II. EXPERIMENTAL DETAILS

A large Tb_5Ge_4 single crystal (~5 grams) was used for the neutron diffraction experiment. The single crystal was grown at the Materials Preparation Center[24] using the Bridgman technique as described in Ref. 25. The mosaic of the crystal is 0.41(3)° along the a axis and 0.63(2)° along the b axis as determined by the full width at half maximum of the (400) and (060) Bragg peak rocking curves. The crystal was mounted on a thin aluminum post, oriented in the $(hk0)$ scattering plane, and sealed in a helium filled aluminum sample can. A closed-cycle Helium refrigerator (Displex) was used which allows accurate temperature control between 10 and 300 K. The experiments were performed using the HB1A triple-axis spectrometer located at the high flux isotope reactor (HFIR) at the Oak Ridge National Laboratory (ORNL). The HB1A spectrometer operates with a fixed incident energy, E_i=14.6 meV using a double pyrolitic graphite (PG) monochromator system. Two highly oriented PG filters were mounted before and after the second monochromator to significantly reduce higher order contaminations of the incident beam (i.e., $I_{\lambda/2} \cong 10^{-4} I_{\lambda}$). A collimation of *open*-40′-sample-40′–68′ was used throughout the experiment. All data have been normalized to the beam monitor count.

III. RESULTS AND DISCUSSIONS

Figure 2 compares longitudinal scans measured along the $(0k0)$ direction at selected temperatures both below [Fig. 2(a)] and above [Fig. 2(b)] T_N. Strong AFM magnetic reflections with k=odd integer were observed below T_N consistent with the magnetic structure of Tb_5Ge_4. At low temperatures, the (010) and (030) magnetic reflections are superimposed on weak and very broad Lorentzian-shaped diffuse scattering peaks arising from magnetic fluctuations. Below T_N, the diffuse scattering increases with increasing temperatures as illustrated in Fig. 2(a). The diffuse scattering is strongest at T_N and then weakens as the temperature increases above T_N as shown in Fig. 2(b) as expected for typical critical behavior. The data indicate strong diffuse scattering around the strong magnetic reflections over a wide temperature range.

We characterized the $T_N \sim 92$ K AFM transition with an order-parameter measurement. Similar results were obtained by monitoring the magnetic reflections (010) and (030). Figure 3(a) depicts the order parameter of Tb_5Ge_4 as measured by monitoring the strong magnetic reflection (030) as a function of temperature. The integrated intensity was obtained by fitting the (030) rocking curve measured at each temperature to a Lorentzian function with a constant background. A fit of the order parameter to a power-law $I(T)=I_0[(T_N-T)/T_N)]^{2\beta}$ yields $T_N \approx 91.38 \pm 0.05$ K and $\beta \approx 0.20 \pm 0.01$, where β is the critical exponent. The fitting result is plotted in Fig. 3(a), solid line, in comparison to calculations using the same fitting parameters but replacing β with the values of a two-dimensional (2D) Ising (β=0.125) and a three-dimensional (3D) Ising (β=0.326) system.[26] The obtained critical temperature T_N is in good agreement with the magnetic susceptibility result. The yielded β value ~0.20 is between the theoretical values of a 2D and a 3D Ising system, which suggests that the magnetic dimensionality of Tb_5Ge_4 is intermediate between 2D and 3D consistent with its layered magnetic structure. The in-plane (along the $(h00)$ direction) and out-of-plane (along the $(0k0)$ direction) correlation lengths were measured by performing relatively wide transverse and longitudinal scans around (030) at several temperatures. The data at each temperature are fit to a Lorentzian, $\propto 1/(q^2+\kappa^2)$, convoluted with Gaussian-shaped instrumental resolution. Here $\kappa=1/\xi$, and ξ is the spin correlation length. The derived correlation lengths along both directions are shown in Fig. 3(b). Similar correlation lengths were obtained along both directions.

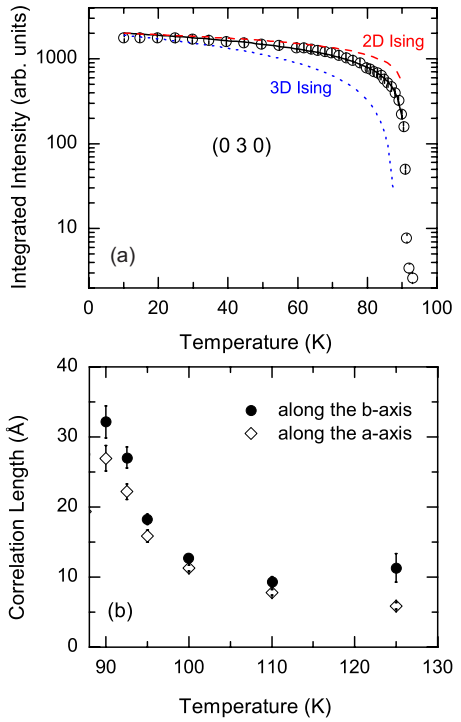

FIG. 3. (Color online) Tb_5Ge_4 order-parameter and spin-correlation lengths. (a) Integrated intensity of the (030) magnetic peak as a function of temperature. The solid line is the fitting of the order-parameter data to the power law as described in the text which yields $T_N \approx 91.38 \pm 0.05$ K and $\beta \approx 0.20 \pm 0.01$, and the dashed and dotted lines are calculations using the same fitting parameters but simply replacing the β value to be the values of a 2D Ising (β=0.125) and a 3D Ising (β=0.326) system. (b) Spin-correlation lengths along the b axis and a axis.

The longitudinal scans shown in Fig. 2 indicate strong diffuse scattering along the b axis. In order to see how the diffuse scattering is distributed in the (hk0) plane, a series of grid scans around (030) were performed at two temperatures, 8 and 88 K. The 8 K data were subtracted from the 88 K data to eliminate contributions from the (030) magnetic Bragg reflection. Figure 4 is the contour plot of the subtracted diffuse scattering intensity vs h and k. It shows that the diffuse scattering extends along both h and k directions. The diffuse scattering intensity is strong around ($\sim$0.1 $\sim$3.10) and its equivalent positions. No strong anisotropy is observed suggesting the magnetic correlations associated to the diffuse scattering are not restricted to the FM block layer (ac plane) but are rather more three-dimensional exhibiting AFM critical scattering behavior.

The diffuse scattering was studied in detail as a function of temperature. Wide transverse scans along the h direction were performed at (0 1.12 0) to reduce contributions from the nearby (010) strong magnetic reflection. At 10 K, the FWHM (full width at half maximum) peak width of the (010) is about 0.09 [r.l.u] (reciprocal lattice unit). Therefore we may attribute the scattering intensity measured at (0 1.12 0) to diffuse scattering from magnetic correlations. Figures 5(a) and 5(b) shows typical scans at different temperatures. The scattering intensity of the strong diffuse scattering peak first increases with increasing temperature up to T_N [Fig. 5(a)] and then decreases with further increasing temperature above T_N [Fig. 5(b)]. In general, the q dependence (here $q = h$ or k) of diffuse scattering can be well described by the following equation,[27,28] a sum of a Lorentzian function and a Squared-Lorentzian function plus constant background (BG),

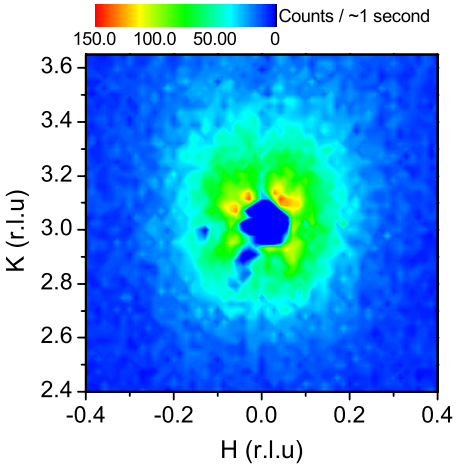

FIG. 4. (Color online) Diffuse scattering intensity (88–8 K) vs k and h around (030) constructed from a series of grid scans measured at 8 and 88 K. The 8 K data is subtracted from the 88 K data to eliminate contributions from (030) magnetic Bragg reflection.

$$\mathcal{I}(q) = \frac{A}{\kappa_L^2 + q^2} + \frac{B}{(\kappa_{LS}^2 + q^2)^2} + BG. \quad (1)$$

The first Lorentzian term is the conventional critical scattering component representing an Ornstein-Zernike form, i.e., $\exp^{-\kappa r}/r$, for the magnetic correlations.[26] The second Squared-Lorentzian term[29] is generally considered to arise from static or frozen spin clusters within which the spin correlations decrease more gradually as $\exp^{-\kappa r}$. Surprisingly, by fitting the data to a Lorentzian+BG function only, a Squared-Lorentzian+BG function only, and the sum of Lorentzian plus Squared-Lorentzian function as described in Eq. (1), respectively, we found that the diffuse scattering data can be best described by the Squared-Lorentzian function only plus constant background. Adding an extra Lorentzian term does not improve the quality of the least-squares fit to data. The comparisons between the fits to a Lorentzian only and a Squared-Lorentzian only are shown in Fig. 5. Note that the diffuse scattering peak is very broad, thus the resolution effect can be neglected and no resolution corrections are applied in the data analysis. Figure 5(c) compares the fits of the 95 K data to Lorentzian+BG (dashed line) only and Squared-Lorentzian+BG (solid line) only. This indicates that the 95 K data cannot be described by a Lorentzian+BG function. On the other hand, as shown in Figs. 5(a) and 5(b), the solid curves are fits to a Squared-Lorentzian+BG only that adequately describe the data for the measured q range at all temperatures. The comparison of the obtained normalized χ^2 from these two fittings is shown in Fig. 5(d). It clearly shows that the data are better captured by a Squared-Lorentzian form, the Lorentzian line shape does not give a good description of the data, particularly at temperatures near T_N as illustrated in Fig. 5(c).

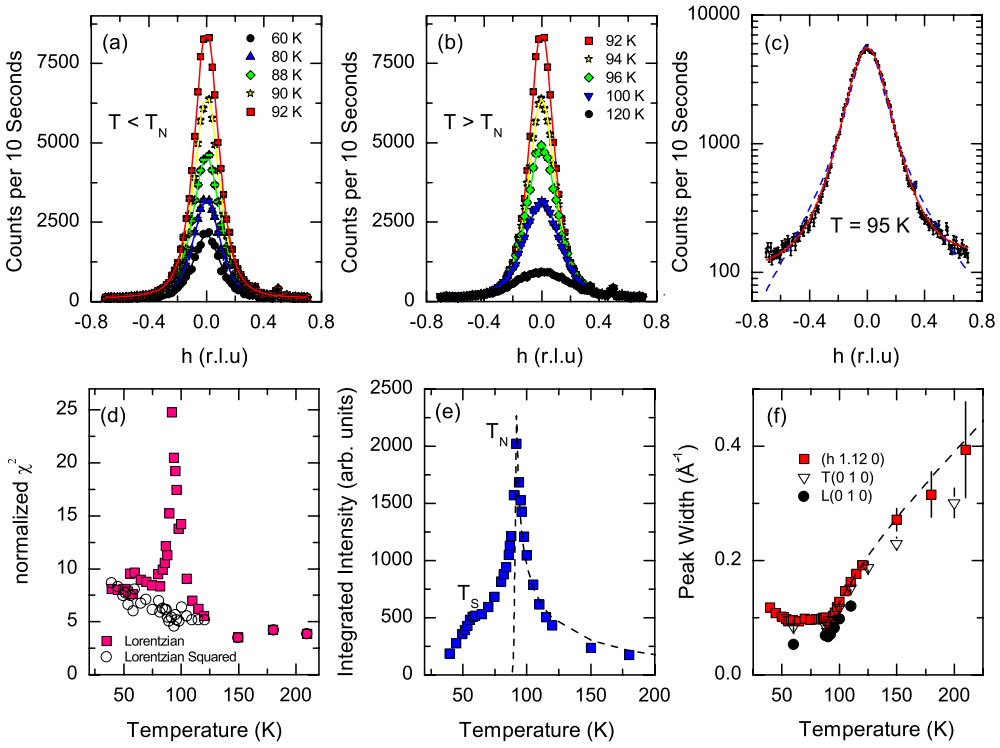

FIG. 5. (Color online) Diffuse scattering along the h direction measured at (0 1.12 0). Representative scans measured at different temperatures (a) below T_N, (b) above T_N. The solid curves are least-squares fits to a Squared-Lorentzian function of h as described in the text; (c) Comparison of the fits of the 95 K data to a Lorentzian+BG (dashed line) function only and a Squared-Lorentzian+BG (solid line) function only; (d) χ^2 vs T, where the normalized χ^2 is obtained from least-squares fits to a Lorentzian+BG only and a Squared-Lorentzian+BG function only; (e) Integrated intensity vs temperature; (f) Peak width vs temperature; The dashed lines in (e) and (f) are fits of the $T>T_N$ data to a power law as described in the text.

The integrated intensity and the FWHM obtained from least-squares fits to the data with a Squared-Lorentzian function are plotted in Figs. 5(e) and 5(f). Two features are observed in the integrated intensity data [Fig. 5(e)]. The small kink at ~55 K is associated with the spin reorientation transition, and the peak at ~92 K is associated with the AFM transition. Both temperatures agree well with the magnetic susceptibility data. Despite the small kink at ~55 K, the ~92 K peak is nearly symmetric indicating strong critical fluctuations at T_N that die off as one moves away from T_N in either direction. Above T_N, the integrated intensity data can be fit to a power law $I(T)=I_0[\ (T-T_N)/T_N)]^{-2\beta'}$ yielding $T_N \approx 90 \pm 1$ K and $\beta' \approx 0.22 \pm 0.02$ [dashed line in Fig. 5(e)]. The obtained β' value agrees to the β value obtained from the fit to the order-parameter data. As illustrated in Fig. 5(f), the correlation length of the SRC remains relatively constant below T_N as indicated by a nearly constant peak width. Above T_N, the peak width increases as expected as the correlation length decreases with increasing temperature. A fit to the $T>T_N$ peak width data to a power law $\xi(T)=\xi_0[\ (T-T_N)/T_N)]^{\upsilon}$ gives $T_N \approx 92 \pm 1$ K and $\upsilon \approx 0.77 \pm 0.06$ [dashed line in Fig. 5(f)], the υ value is between the theoretical values of a 3D Ising (υ=0.6312) and a 2D Ising (υ=1) (Ref. 26) consistent with the order-parameter measurement results. The Squared-Lorentzian peak widths obtained from fits to (010) longitudinal and transverse scans are also shown in Fig. 5(f). The Lorentzian-squared lineshape provides the best fit along both the h and k directions, indicating that the correlations in the spin clusters extend both in the block layers and between the blocks.

Our neutron diffraction study reveals strong diffuse scattering in Tb_5Ge_4 that persists to temperatures well above T_N. A detailed study of the peak shape indicates it is not conventional critical scattering with a Lorentzian shape but shows a Squared-Lorentzian peak shape. As described in Refs. 29 and 30, the Squared-Lorentzian term arises if the pair correlation function falls off as $\exp^{-\kappa r}$, which is characteristic of a spin-cluster state. Although the diffuse scattering is Squared-Lorentzian in form providing evidence of a clustered magnetic state in Tb_5Ge_4, we believe that the diffuse scattering observed in Tb_5Ge_4 is quite different from the proposed FM Griffiths-like phase in Gd_5Ge_4 (inferred from dc/ac magnetization and magnetic susceptibility studies)[12] for the following reasons. (1) As depicted in Fig. 2, at temperatures both below and above T_N, the diffuse scattering is peaked at odd values of k (AFM wave vector) only, indicating that it is associated with AFM fluctuations. (2) The integrated intensity of the diffuse scattering also behaves like that typical of magnetic critical fluctuations, with a divergence of the correlation length at T_N. (3) The critical exponents obtained by fits of the diffuse scattering integrated intensity and peak width to a power law are consistent with the values obtained from AFM order parameter measurements. (4) Quasielastic measurements indicate the diffuse scattering is static in origin. Our neutron diffraction data indicate that the diffuse scattering observed in Tb_5Ge_4 exhibits behaviors of AFM

critical fluctuations despite the Squared-Lorentzian peak shape.

The fact that the peak shape of the diffuse scattering is not a Lorentzian, as expected for normal critical scattering, is interesting and should not be left without a discussion. Here we consider two possibilities that may affect the diffuse scattering peak shape. (1) The Squared-Lorentzian peak shape may be intrinsic, i.e., related to the Griffiths-like phase, formation of which has been discussed in Refs. 12 and 16; (2) The unusual peak shape may also arise from some extrinsic effects, for example impurities in Tb_5Ge_4. It has been reported that $R_5(Si_xGe_{1-x})_3$-type impurity phases, seen as very thin plates that are scattered through the bulk of $R_5(Si_xGe_{1-x})_4$ samples, are present in all studied compounds of this series regardless of R.[31] Our data show that Tb_5Ge_3 impurity phase is also present in the studied Tb_5Ge_4 crystal. It is possible that the Tb magnetic sublattices of Tb_5Ge_4 are disrupted by the Tb_5Ge_3 impurities resulting in spin-clusters in Tb_5Ge_4 which give rise to the squared-Lorentzian diffuse scattering peak shape.

ACKNOWLEDGMENTS

Ames Laboratory is operated for the U.S. Department of Energy by Iowa State University under Contract No. DE-AC02-07CH11358. The HFIR is a national user facility funded by the United States Department of Energy, Office of Basic Energy Sciences, Materials Science, under Contract No. DE-AC05-00OR22725 with UT-Battelle, LLC.

[1] V. K. Pecharsky and K. A. Gschneidner, Jr., Phys. Rev. Lett. **78**, 4494 (1997).
[2] V. K. Pecharsky and K. A. Gschneidner, Jr., Appl. Phys. Lett. **70**, 3299 (1997).
[3] V. K. Pecharsky and K. A. Gschneidner, Jr., J. Magn. Magn. Mater. **167**, L179 (1997).
[4] V. K. Pecharsky and K. A. Gschneidner, Jr., J. Alloys Compd. **260**, 98 (1997).
[5] V. K. Pecharsky and K. A. Gschneidner, Jr., Adv. Cryog. Eng. **43**, 1729 (1998).
[6] G. J. Miller, Chem. Soc. Rev. **35**, 799 (2006).
[7] L. Morellon, C. Magen, P. A. Algarabel, M. R. Ibarra, and C. Ritter, Appl. Phys. Lett. **79**, 1318 (2001).
[8] F. Casanova, A. Labarta, and X. Batlle, Phys. Rev. B **72**, 172402 (2005).
[9] H. Tang, V. K. Pecharsky, K. A. Gschneidner, Jr., and A. O. Pecharsky, Phys. Rev. B **69**, 064410 (2004).
[10] E. M. Levin, K. A. Gschneidner, Jr., and V. K. Pecharsky, Phys. Rev. B **65**, 214427 (2002).
[11] Z. W. Ouyang, V. K. Pecharsky, K. A. Gschneidner, Jr., D. L. Schlagel, and T. A. Lograsso, Phys. Rev. B **74**, 024401 (2006).
[12] Z. W. Ouyang, V. K. Pecharsky, K. A. Gschneidner, Jr., D. L. Schlagel, and T. A. Lograsso, Phys. Rev. B **74**, 094404 (2006).
[13] E. M. Levin, K. A. Gschneidner, Jr., T. A. Lograsso, D. L. Schlagel, and V. K. Pecharsky, Phys. Rev. B **69**, 144428 (2004).
[14] C. Magen, Z. Arnold, L. Morellon, Y. Skorokhod, P. A. Algarabel, M. R. Ibarra, and J. Kamarad, Phys. Rev. Lett. **91**, 207202 (2003).
[15] C. Ritter, L. Morellon, P. A. Algarabel, C. Magen, and M. R. Ibarra, Phys. Rev. B **65**, 094405 (2002).
[16] C. Magen, P. A. Algarabel, L. Morellon, J. P. Araújo, C. Ritter, M. R. Ibarra, A. M. Pereira, and J. B. Sousa, Phys. Rev. Lett. **96**, 167201 (2006).
[17] P. Schobinger-Papamantellos, J. Phys. Chem. Solids **39**, 197 (1978).
[18] L. Tan, A. Kreyssig, J. W. Kim, A. I. Goldman, R. J. McQueeney, D. Wermeille, B. Sieve, T. A. Lograsso, D. L. Schlagel, S. L. Budko, V. K. Pecharsky, and K. A. Gschneidner, Jr., Phys. Rev. B **71**, 214408 (2005).
[19] L. Tan, Ph.D. thesis, Iowa State University (2008).
[20] R. B. Griffiths, Phys. Rev. Lett. **23**, 17 (1969).
[21] J. Deisenhofer, D. Braak, H.-A. Krug von Nidda, J. Hemberger, R. M. Eremina, V. A. Ivanshin, A. M. Balbashov, G. Jug, A. Loidl, T. Kimura, and Y. Tokura, Phys. Rev. Lett. **95**, 257202 (2005).
[22] M. B. Salamon, P. Lin, and S. H. Chun, Phys. Rev. Lett. **88**, 197203 (2002).
[23] M. C. de Andrade, R. Chau, R. P. Dickey, N. R. Dilley, E. J. Freeman, D. A. Gajewski, M. B. Maple, R. Movshovich, A. H. Castro Neto, G. Castilla, and B. A. Jones, Phys. Rev. Lett. **81**, 5620 (1998).
[24] Single-crystals synthesized at the Materials Preparation Center, Ames Laboratory, US DOE Basic Energy Sciences, Ames, IA, USA: www.mpc.ameslab.gov
[25] T. A. Lograsso, D. L. Schlagel, and A. O. Pecharsky, J. Alloys Compd. **393**, 141 (2005).
[26] F. Malcolm, *Collins* (Magnetic Critical Scattering, New York, 1989).
[27] K. Motoya and K. Hioki, J. Phys. Soc. Jpn. **72**, 930 (2003).
[28] P. Bentley, J. R. Stewart, and R. Cywinski, Appl. Phys. A: Mater. Sci. Process. **74**, S862 (2002).
[29] S. W. Lovesey, J. Phys. C **17**, L213 (1984).
[30] *Methods of Experimental Physics*, Vol. 23, *Neutron Scattering* part C, edited by Kurt Sköld and David L. Price (Academic, New York, 1987).
[31] O. Ugurlu, L. S. Chumbley, D. L. Schlagel, and T. A. Lograsso, Acta Mater. **54**, 1211 (2006).